Energy 91 (2015) 72–83

Contents lists available at ScienceDirect

Energy

journal homepage: www.elsevier.com/locate/energy

Entropy generation in a micropolar fluid flow through an inclined channel with slip and convective boundary conditions

D. Srinivasacharya*, K. Hima Bindu

Department of Mathematics, National Institute of Technology, Warangal 506004, India

ARTICLE INFO

Article history:
Received 4 June 2015
Received in revised form
5 August 2015
Accepted 8 August 2015
Available online 3 September 2015

Keywords:
Slip flow
Micropolar fluid
Convective boundary condition
Inclined channel
Entropy
Bejan number

ABSTRACT

The present paper studies the entropy generation in a micropolar fluid flow through an inclined channel with slip and convective boundary conditions. The governing equations are linearized using quasi-linearization and then solved using Chebyshev spectral collocation method. The velocity, micro-rotation and temperature profiles are obtained and utilized to compute entropy generation and Bejan number. The effects of the angle of inclination, coupling number, slip parameter, Biot number and Brinkman number on the velocity, microrotation, temperature, entropy generation and Bejan number are studied and presented graphically. The results reveal that the entropy generation number increases with the increase of angle of inclination and Brinkman number while the increase of coupling number and Reynolds number causes the entropy generation to reduce. It is observed that the heat transfer irreversibility dominates at the centre of the channel.

1. Introduction

The optimal design criteria for thermal systems by minimizing their entropy generation have recently been a topic of great interest. Efficient utilization of energy is the main objective in the design of thermal devices. The performance of thermal devices is always affected by irreversible losses that lead to an increase of entropy and reduce the thermal efficiency. Therefore, in the energy optimization problems and design of many traditional heat removal engineering devices, it is necessary to minimize the entropy generation or destruction of available work due to heat transfer and fluid friction as a function of the design variables selected for the optimization analysis. The entropy generation is encountered in many energy related applications, such as solar power collectors, geothermal energy systems and the cooling of modern electronic systems. Entropy generation analysis provides a useful tool to identify the irreversibilities in any thermal system as well as to determine the optimum condition for any process. A variety of fluid flow systems have been analyzed and optimized using the EGM (entropy generation minimization) method. Several investigations ([1–6]) were carried on entropy generation under various flow configurations.

Fluid flow and heat transfer inside channels with simple geometry and different boundary conditions is one of the fundamental areas of research in engineering. It has wide range of thermal engineering applications in electronics cooling, thermal insulation engineering, water movement in geothermal reservoirs, heat pipes and thermal insulation. Recently, a wide literature on fluid flow and entropy generation in various channels has been developed. Havzali et al. [7] investigated the effect of entropy generation on a laminar, viscous, incompressible flow between two inclined, parallel, isothermal plates. They observed that the entropy generation in a small section is dominant on the total entropy production. Kamisli and Oztop [8] examined the entropy generation in two immiscible incompressible fluid flows under the influence of pressure difference in thin slit of constant wall heat fluxes. Cimpean and Pop [9] studied the entropy generation for a mixed convection flow of a fluid saturated porous medium through an inclined channel with uniform heated walls. Komurgoz et al. [10] investigated the magnetic effect on heat-fluid and entropy generation interactions in an inclined channel consisting of two regions: one filled with clear fluid and the second with porous medium. Damseh et al. [11] studied the local entropy generation due to steady fully developed laminar forced convection channel flow in the presence of a transverse magnetic field. Eegunjobi and Makinde

* Corresponding author.
E-mail addresses: dsc@nitw.ac.in, dsrinivasacharya@yahoo.com (D. Srinivasacharya).

http://dx.doi.org/10.1016/j.energy.2015.08.014
0360-5442/

Nomenclature

a_j	microinertia parameter
B_e	Bejan number
Bi	Biot number
B_r	Brinkman number
C_p	specific heat
f	dimensionless velocity
Gr	Grashof number
$2h$	channel width
K_f	thermal conductivity
m^2	micropolar parameter
N	coupling number
N_h	entropy generation due to heat transfer
N_ϑ	entropy generation due to viscous dissipation
N_s	dimensionless entropy generation number
Re	Reynolds number
T	Dimensional Temperature
T_1	ambient Temperature
T_2	fluid Temperature
u	dimensional axial velocity
X	horizontal axis (direction of flow)
Y	coordinate perpendicular to the plate

Greek Symbols

α	inclined angle
α_1	slip parameter
β,γ	gyration viscosity coefficients
θ	dimensionless temperature
κ	vortex viscosity
μ	viscosity of the fluid
ρ	density of the fluid
σ	dimensionless microrotational component

[12] presented combined effects of variable viscosity and asymmetric convective boundary conditions on the entropy generation rate in MHD porous channel flow. Das and Jana [13] investigated the combined effects of magnetic field, suction/injection and Navier slips on entropy generation in an MHD flow through a porous channel under a constant pressure gradient. Mahdavi et al. [14] investigated the entropy generation and convective heat transfer of a pipe partially filled with a porous material by numerical simulation. Torbabi et al. [15] studied the heat transfer and entropy generation in a channel partially filled with porous media using local thermal non-equilibrium model. They discussed about the effects of many thermophysical parameters on the velocity, temperature, Nusselt number and entropy generation rates. Torabi and Zhang [16] analyzed the local and total entropy generation in MHD porous channel with thick walls.

The fluids with slip velocity have many applications at both macro and micro scales in technology such as polishing of surfaces and in micro devices. Navier [17] proposed a slip boundary condition where the slip velocity depends linearly on the shear stress. At macro level, wall slip is encountered in polymer extrusion processes where it is caused by instabilities at high stress levels [18]. Denn [19] presented a review of mechanisms of slip in non-Newtonian fluids and also explores the relation between slip and extrusion instabilities. Also the study of convective heat transfer has much importance in high-temperature processes like gas turbines, nuclear plants, thermal energy storage, etc. The effects of slip velocity and convective heat transfer on entropy generation for any fluid flow of different geometries have been studied by several authors. Iman [20] investigated the importance of thermal boundary conditions of the heated/cooled walls in the development of flow, heat transfer, and observed the characteristics of entropy generation in a porous enclosure. Hooman [21] presented the effect of velocity slip, temperature jump, and duct geometry on heat transfer and entropy generation through a micro duct of rectangular cross-section. Butt et al. [22] presented the effects of hydrodynamic slip on entropy generation in a viscous flow over a vertical plate with convective boundary condition. Chinyoka and Makinde [23] investigated the entropy generation rate in an unsteady porous channel flow with Navier slip subjected to asymmetrical convective boundary conditions. Anand [24] discussed the effect of slip on the entropy generation and heat transfer characteristics of the fully developed flows of power law fluids in a micro channel. Mostafa and Ali [25] presented the analytical solution for non-Newtonian fluid flows between parallel-plates in micro scale subject to iso-flux and isothermal wall boundary conditions, while taking the effects of wall slip and viscous dissipation into consideration. Ibanez [26] studied the combined effects of hydrodynamic slip, magnetic field and suction/injection Reynolds number on the global entropy generation rate under convective boundary conditions.

Most of the researchers have reported their study on entropy generation pertaining to viscous fluid. The study of viscous fluid does not adequately describe the flow properties of polymeric fluids, animal blood, coal slurries, Mine tailings and mineral suspensions. Such properties are described in non-Newtonian fluid flow model. Many fluids in nature and industrial processes show a non-Newtonian fluid behavior. One among those models is micropolar fluid introduced by Eringen [27] which exhibit certain microscopic effects arising from the local structure and microrotations of fluid elements. The Micropolar fluids have been shown to accurately simulate the flow characteristics of polymeric additives, geomorphological sediments, colloidal suspensions, haematological suspensions, liquid crystals, lubricants, etc. The main advantage of using micropolar fluid model compared to other non-Newtonian fluids is that it takes care of the rotation of fluid particles by means of an independent kinematic vector called the microrotation vector.

The majority of the studies reported in the literature on entropy generation analysis for micropolar fluid flows deal with horizontal channel subject to thermal and/or wall flux boundary conditions. However, in the present analysis an attempt is made to analyze the effect of angle of inclination of the channel, slip velocity and convective boundary conditions on entropy generation in a micropolar fluid flow through an inclined channel. The velocity, microrotation and the temperature distribution are determined by solving the momentum, angular momentum and energy equations with Spectral Quasi linearization method. The obtained velocity, microrotation and the temperature distribution are utilized to compute the entropy generation and Bejan number.

2. Mathematical formulation

Consider a steady laminar incompressible fully developed micropolar fluid flow bounded by two infinite inclined parallel plates separated by a distance $2h$. The channel is inclined at an angle α. Choose the cartesian coordinate system with x-axis aligned at the center of the channel in the direction of the flow and the y-axis perpendicular to the plates (as shown in Fig. 1). Since the

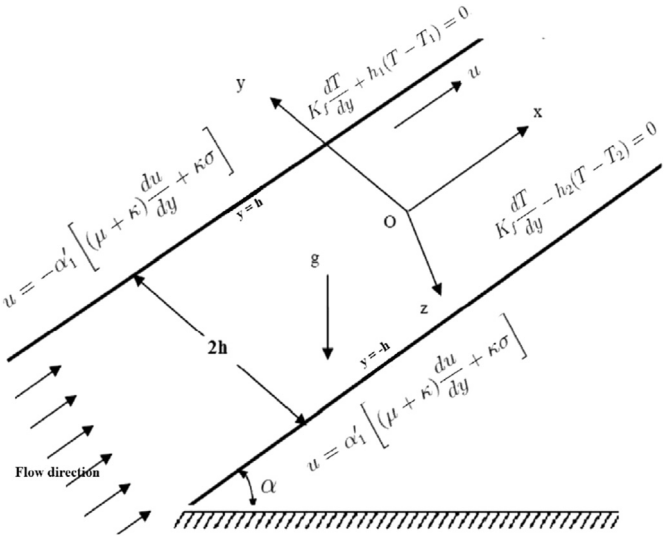

Fig. 1. Schematic diagram of the problem.

boundaries in the x direction are of infinite dimensions. Without loss of generality, we assume that the physical quantities depend on y only. The fluid properties are assumed to be constant except for density variations in the buoyancy force term. The fluid velocity vector $\overline{q} = (u; v)$ is assumed to be parallel to the x-axis, so that only the x component u of the velocity vector does not vanish but the transpiration cross-flow velocity v_0 remains constant, where $v_0 < 0$ is the velocity of suction and $v_0 > 0$ is the velocity of injection.

With the above assumptions and Boussinesq approximations, the equations governing the flow of steady incompressible micropolar fluid are:

$$v = v_0 \tag{1}$$

$$(\mu+\kappa)\frac{d^2u}{dy^2} - \rho v_0\frac{du}{dy} + \kappa\frac{d\sigma}{dy} + \rho g^*\beta(T-T_1)\sin(\alpha) - \frac{\partial p}{\partial x} = 0 \tag{2}$$

$$\gamma\frac{d^2\sigma}{dy^2} - \rho j^* v_0\frac{d\sigma}{dy} - 2\kappa\sigma - \kappa\frac{du}{dy} = 0 \tag{3}$$

$$K_f\frac{d^2T}{dy^2} - \rho C_p v_0\frac{dT}{dy} + (\mu+\kappa)\left(\frac{du}{dy}\right)^2 + 2\kappa\left(\sigma^2 + \sigma\frac{du}{dy}\right) + \gamma\left(\frac{d\sigma}{dy}\right)^2 = 0 \tag{4}$$

where u is velocity component in the x direction, σ is microrotation, ρ and j^* are the fluid density and gyration parameter, μ, κ and γ are the material constants (viscosity coefficients), g^* is the acceleration due to gravity, p is pressure, β is the coefficient of thermal expansion, K_f is the thermal conductivity.

The following slip, no-spin and convective boundary conditions are proposed

$$u = -\alpha_1'\left[(\mu+\kappa)\frac{du}{dy} + \kappa\sigma\right], \quad \sigma = 0, \quad K_f\frac{dT}{dy} + h_1(T-T_1) = 0, \quad \text{at} \quad y = h \tag{5a}$$

$$u = \alpha_1'\left[(\mu+\kappa)\frac{du}{dy} + \kappa\sigma\right], \quad \sigma = 0, \quad K_f\frac{dT}{dy} - h_2(T-T_2) = 0, \quad \text{at} \quad y = -h \tag{5b}$$

where α_1' is the slip length of the upper and lower plates of the channel, T is the temperature, T_1 is the ambient temperature, T_2 is the hot fluid temperature, K_f fluid thermal conductivity and h_1,h_2 are the convective heat transfer coefficients for each plate.

Introducing the following dimensionless quantities:

$$\eta = \frac{y}{h}, \quad u = U_0 f(\eta), \quad \sigma = \frac{U_0}{h}g(\eta), \quad \theta(\eta) = \frac{T-T_1}{T_2-T_1}, \quad \overline{\alpha_1} = \frac{\alpha_1'}{h} \tag{6}$$

in Equations (1)–(4), we get the following non-linear system of differential equations:

$$\frac{1}{1-N}f''' - Rf' + \frac{N}{1-N}g' + \frac{Gr}{Re}\sin(\alpha)\theta = A \tag{7}$$

$$\frac{2-N}{m^2}g'' - a_j R\left(\frac{1-N}{N}\right)g' - 2g - f' = 0 \tag{8}$$

$$\theta'' - RPr\theta' + \frac{Br}{1-N}\left[f'^2 + 2N\left(g^2 + gf'\right) + \frac{N(2-N)}{m^2}g'^2\right] = 0 \tag{9}$$

where primes denote differentiation with respect to η, $Pr = \frac{\mu C_p}{K_f}$ is the Prandtl number, $Re = \frac{\rho U_0 h}{\mu}$ is the Reynolds number, $R = \frac{\rho v_0 h}{\mu}$ is the suction/injuction parameter, $N = \frac{\kappa}{\kappa+\mu}$ is the coupling number, $Gr = \frac{\rho^2 g\beta(T_2-T_1)h^3}{\mu^2}$ is the Grashof number, $A = \frac{h^2}{\mu U0}\frac{dp}{dx}$ is the constant pressure gradient, $m^2 = \frac{h^2\kappa(2\mu+\kappa)}{\gamma(\mu+\kappa)}$ is the micropolar parameter, $a_j = \frac{j^*}{h^2}$ is the micro-inertia parameter, $Br = \frac{\mu U_0^2}{K_f(T_2-T_1)}$ is the Brinkman number.

The corresponding boundary conditions are:

$$f = -\frac{\alpha_1}{1-N}f', \quad g = 0, \quad \theta' + Bi_1\theta = 0, \quad \text{at} \quad \eta = 1 \tag{10a}$$

$$f = \frac{\alpha_1}{1-N}f', \quad g = 0, \quad \theta' - Bi_2\theta = -Bi_2, \quad \text{at} \quad \eta = -1 \tag{10b}$$

where $\alpha_1 = \overline{\alpha_1}\mu$ is the slip coefficient, $Bi_i = \frac{hh_i}{K_f}$ is the Biot number for each plate. Subindexes $i = 1,2$ refer to the lower and upper plates, respectively. In general Biot number assumed to be same for the lower and upper plates.

3. Method of solution

The system of Equations (7)–(9) along with the boundary conditions (10) are solved using the quasilinearization method. This quasilinearization method (QLM) is a generalization of the Newton–Raphson method and was proposed by Bellman and Kalaba [28] for solving nonlinear boundary value problems. In this method the iteration scheme is obtained by linearizing the nonlinear component of a differential equation using the Taylor series expansion.

Let the f_r, g_r and θ_r be an approximate current solution and f_{r+1}, g_{r+1} and θ_{r+1} be an improved solution of the system of Equations (7)–(9). By taking Taylors series expansion of non-linear terms in

(7)–(9) around the current solution and neglecting the second and higher order derivative terms, we get the linearized equations as:

$$\frac{1}{1-N}f''_{r+1} - Rf'_{r+1} + \frac{N}{1-N}g'_{r+1} + \frac{Gr}{Re}\sin(\alpha)\theta_{r+1} = A \tag{11}$$

$$\frac{2-N}{m^2}g''_{r+1} - a_jR\left(\frac{1-N}{N}\right)g'_{r+1} - 2g_{r+1} - f'_{r+1} = 0 \tag{12}$$

$$\theta''_{r+1} - RPr\theta'_{r+1} + a_{1,r}f'_{r+1} + a_{2,r}g'_{r+1} + a_{3,r}g_{r+1} = a_{4,r} \tag{13}$$

where the coefficients $a_{s,r}s = 1,2,\ldots$ are known functions calculated from previous iterations and are defined as

$$\left.\begin{aligned} a_{1,r} &= \frac{2Br}{1-N}\left[f'_r + Ng_r\right], \quad a_{2,r} = \frac{2Br}{1-N}\frac{N(2-N)}{m^2}g'_r, \quad a_{3,r} = \frac{2BrN}{1-N}\left[f'_r + 2g_r\right], \\ a_{4,r} &= \frac{Br}{1-N}\left[f'^2_r + 2N\left(g^2_r + g_rf'_r\right) + \frac{N(2-N)}{m^2}g'^2_r\right] \end{aligned}\right\} \tag{14}$$

The above linearized Equations (11)–(13) are solved using the Chebyshev spectral collocation method [29]. The unknown functions are approximated by the Chebyshev interpolating polynomials in such a way that they are collocated at the Gauss-Lobatto points defined as

$$\xi_j = \cos\frac{\pi j}{J}, \quad j = 0,1,2,\ldots,J \tag{15}$$

where J is the number of collocation points used.

The functions f_{r+1}, g_{r+1} and θ_{r+1} are approximated at the collocation points by

$$\left.\begin{aligned} f_{r+1}(\xi) &= \sum_{k=0}^{J} f_{r+1}(\xi_k)T_k(\xi_j), \quad g_{r+1}(\xi) = \sum_{k=0}^{J} g_{r+1}(\xi_k)T_k(\xi_j), \\ \theta_{r+1}(\xi) &= \sum_{k=0}^{J} \theta_{r+1}(\xi_k)T_k(\xi_j) \quad j = 0,1,2,\ldots\ldots,J \end{aligned}\right\} \tag{16}$$

where T_k is the k^{th} Chebyshev polynomial defined by

$$T_k(\xi) = \cos\left[k\cos^{-1}\xi\right] \tag{17}$$

The derivatives of the variables at the collocation points are represented as

$$\left.\begin{aligned} \frac{d^af_{r+1}}{d\eta^a} &= \sum_{k=0}^{J}\mathbf{D}^a_{kj}f_{r+1}(\xi_k), \quad \frac{d^ag_{r+1}}{d\eta^a} = \sum_{k=0}^{J}\mathbf{D}^a_{kj}g_{r+1}(\xi_k), \\ \frac{d^a\theta_{r+1}}{d\eta^a} &= \sum_{k=0}^{J}\mathbf{D}^a_{kj}\theta_{r+1}(\xi_k), \quad j = 0,1,2,\ldots\ldots,J. \end{aligned}\right\} \tag{18}$$

where a is the order of differentiation and $\mathbf{D}$ being the Chebyshev spectral differentiation matrix. Substituting Equations (16)–(18) into Equations (11)–(13) leads to the matrix equation

$$\mathbf{A}_r\mathbf{X}_{r+1} = \mathbf{B}_r, \tag{19}$$

In Equation (19), $\mathbf{A}_r$ is a $(3J+3)\times(3J+3)$ square matrix and $\mathbf{X}_{r+1}$ and $\mathbf{B}_r$ are $(3J+3)\times 1$ column vectors defined by

$$\mathbf{A}_r = \begin{bmatrix} A_{11} & A_{12} & A_{13} \\ A_{21} & A_{22} & A_{23} \\ A_{31} & A_{32} & A_{33} \end{bmatrix}, \quad \mathbf{X}_{r+1} = \begin{bmatrix} \mathbf{F}_{r+1} \\ \mathbf{G}_{r+1} \\ \Theta_{r+1} \end{bmatrix}, \quad \mathbf{R}_r = \begin{bmatrix} \mathbf{r}_{1,r} \\ \mathbf{r}_{2,r} \\ \mathbf{r}_{3,r} \end{bmatrix} \tag{20}$$

where

$$\left.\begin{aligned} \mathbf{F}_{r+1} &= \left[f_{r+1}(\xi_0), f_{r+1}(\xi_1), \ldots\ldots, f_{r+1}(\xi_{J-1}), f_{r+1}(\xi_J)\right]^T, \\ \mathbf{G}_{r+1} &= \left[g_{r+1}(\xi_0), g_{r+1}(\xi_1), \ldots\ldots, g_{r+1}(\xi_{J-1}), g_{r+1}(\xi_J)\right]^T, \\ \Theta_{r+1} &= \left[\theta_{r+1}(\xi_0), \theta_{r+1}(\xi_1), \ldots\ldots, \theta_{r+1}(\xi_{J-1}), \theta_{r+1}(\xi_J)\right]^T, \\ A_{11} &= \frac{1}{1-N}\mathbf{D}^2 - R\mathbf{D}, \quad A_{12} = \left(\frac{N}{1-N}\right)\mathbf{D}, \quad A_{13} = \frac{Gr}{Re}\sin\alpha\mathbf{I}, \\ A_{21} &= -\mathbf{D}, \quad A_{22} = \frac{2-N}{m^2}\mathbf{D}^2 - a_jR\left(\frac{1-N}{N}\right)\mathbf{D} - 2\mathbf{I}, \quad A_{23} = \mathbf{0}, \\ A_{31} &= a_{1,r}\mathbf{D}, \quad A_{32} = a_{2,r}\mathbf{D} + a_{3,r}\mathbf{I}, \quad A_{33} = \mathbf{D}^2 - RPr\mathbf{D}, \\ \mathbf{r}_{1,r} &= A, \mathbf{r}_{2,r} = \mathbf{0_1}, \mathbf{r}_{3,r} = a_{4,r}. \end{aligned}\right\} \tag{21}$$

Here $\mathbf{I}$, $\mathbf{0}$ represents $(J+1)\times(J+1)$ identity matrix, zero matrix respectively.

The corresponding boundary conditions

$$\left.\begin{aligned} f_{r+1}(\xi_0) &= -\frac{\alpha_1}{1-N}\sum_{k=0}^{J}\mathbf{D}_{0k}f_{r+1}(\xi_k), \quad g_{r+1}(\xi_0) = 0, \\ \sum_{k=0}^{J}\mathbf{D}_{0k}\theta_{r+1}(\xi_k) &+ Bi\theta_{r+1}(\xi_0) = 0 \\ f_{r+1}(\xi_J) &= \frac{\alpha_1}{1-N}\sum_{k=0}^{J}\mathbf{D}_{Jk}f_{r+1}(\xi_k), \quad g_{r+1}(\xi_J) = 0, \\ \sum_{k=0}^{J}\mathbf{D}_{Jk}\theta_{r+1}(\xi_k) &- Bi\theta_{r+1}(\xi_J) = -Bi \end{aligned}\right\} \tag{22}$$

After modifying the matrix system (19) to incorporate boundary conditions (22), the solution is obtained as

$$\mathbf{X}_{r+1} = \mathbf{A}_r^{-1}\mathbf{B}_r \tag{23}$$

The initial approximations f_0, g_0 and θ_0 are chosen to be functions that satisfies the boundary conditions (22) i.e.

$$f_0(\eta) = 0, \quad g_0(\eta) = 0, \quad \theta_0(\eta) = 0.5 - 0.5\frac{Bi}{1+Bi}\eta \tag{24}$$

4. Entropy generation

The volumetric rate of entropy generation for incompressible micropolar fluid given as

$$S_G = \frac{K_f}{T_1^2}\left(\frac{dT}{dy}\right)^2 + \frac{\mu+\kappa}{T_1}\left(\frac{du}{dy}\right)^2 + \frac{2\kappa}{T_1}\left[\sigma^2 + \sigma\frac{du}{dy}\right] + \frac{\gamma}{T_1}\left(\frac{d\sigma}{dy}\right)^2$$

According to Bejan [3], the dimensionless entropy generation number N_s is the ratio of the volumetric entropy generation rate to the characteristic entropy generation rate. Thus the entropy generation number is given by

$$N_s = \theta'^2 + \frac{Br}{T_p}\left[\frac{1}{1-N}f'^2 + \frac{2N}{1-N}\left(g^2 + gf'\right) + \frac{N(2-N)}{m^2(1-N)}g'^2\right] \tag{25}$$

where $T_p = \frac{\Delta T}{T_1}$ is the dimensionless temperature difference, and the characteristic entropy generation rate is $\frac{K_f(\Delta T)^2}{h^2 T_1^2}$. The Equation (25) can be expressed alternatively as follows

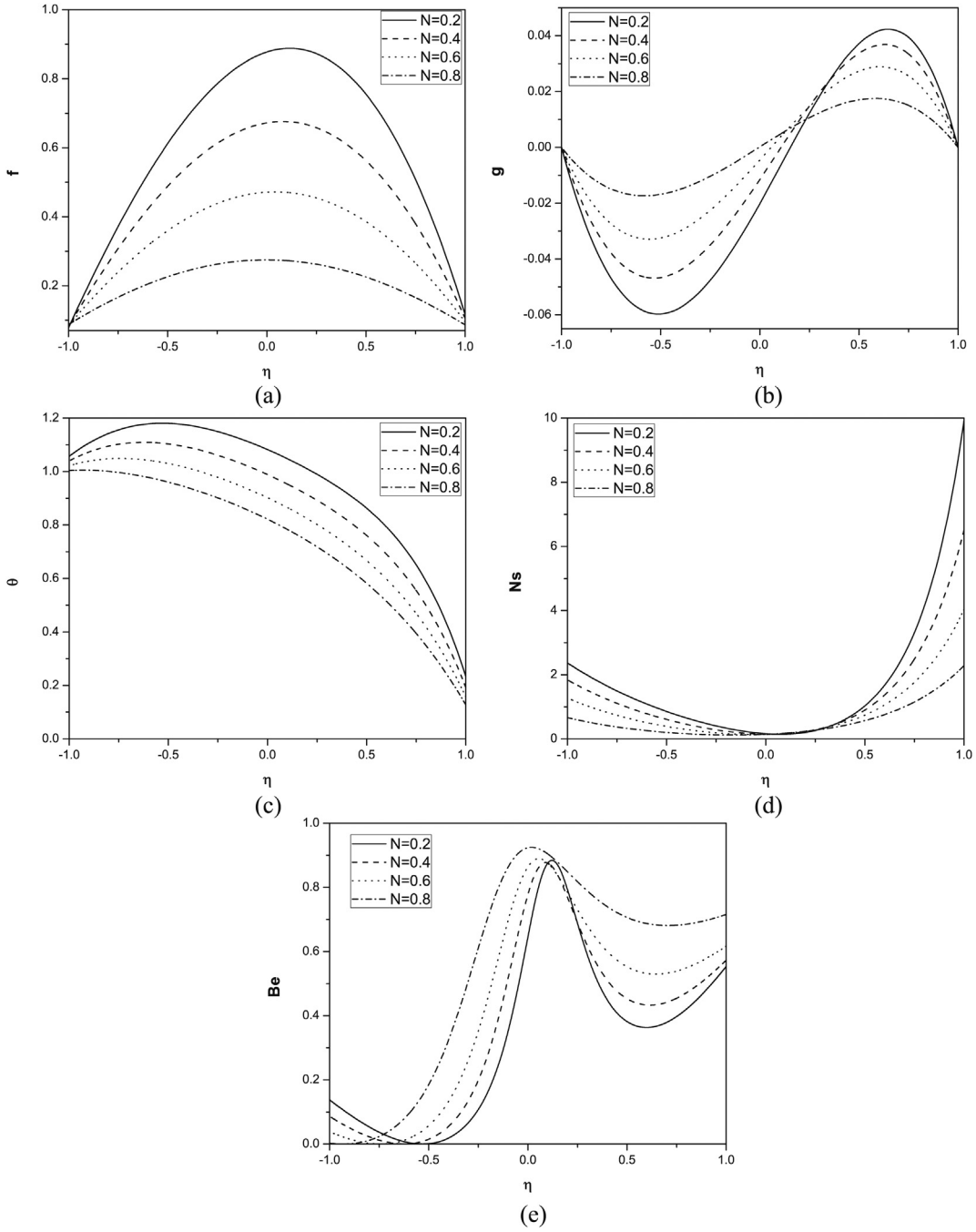

Fig. 2. Effect of coupling number on velocity, microrotation, temperature, entropy generation and Bejan number for $Pr = 1$, $a_j = 0.001$, $Bi = 10$, $A = -1$, $\alpha_1 = 0.05$, $Re = 1$, $Br = 1$, $\alpha = \pi/6$, $m = 1$, $Gr = 2$, $T_p = 1$, $R = 1$.

$$N_s = N_h + N_v \tag{26}$$

The first term on the right hand side of this equation denotes the entropy generation due to heat transfer irreversibility and the second term represents the entropy generation due to viscous dissipation.

To evaluate the irreversibility distribution, the parameter *Be* (Bejan number), which is the ratio of entropy generation due to heat transfer to the overall entropy generation (26) is defined as follows

$$Be = \frac{N_h}{N_h + N_v} \tag{27}$$

The Bejan number varies from 0 to 1. Subsequently, $Be = 0$ reveals that the irreversibility due to viscous dissipation dominates, whereas $Be = 1$ indicates that the irreversibility due to heat transfer is dominant. It is obvious that the $Be = 0.5$ is the case in which the irreversibility due to heat transfer is equal to viscous dissipation.

5. Results and discussion

The solutions for the dimensionless velocity, microrotation, temperature, entropy generation and Bejan number are computed and shown graphically in Figs. 2 to 7. The effects of coupling number N, angle of inclination α, slip parameter α_1, Brinkman

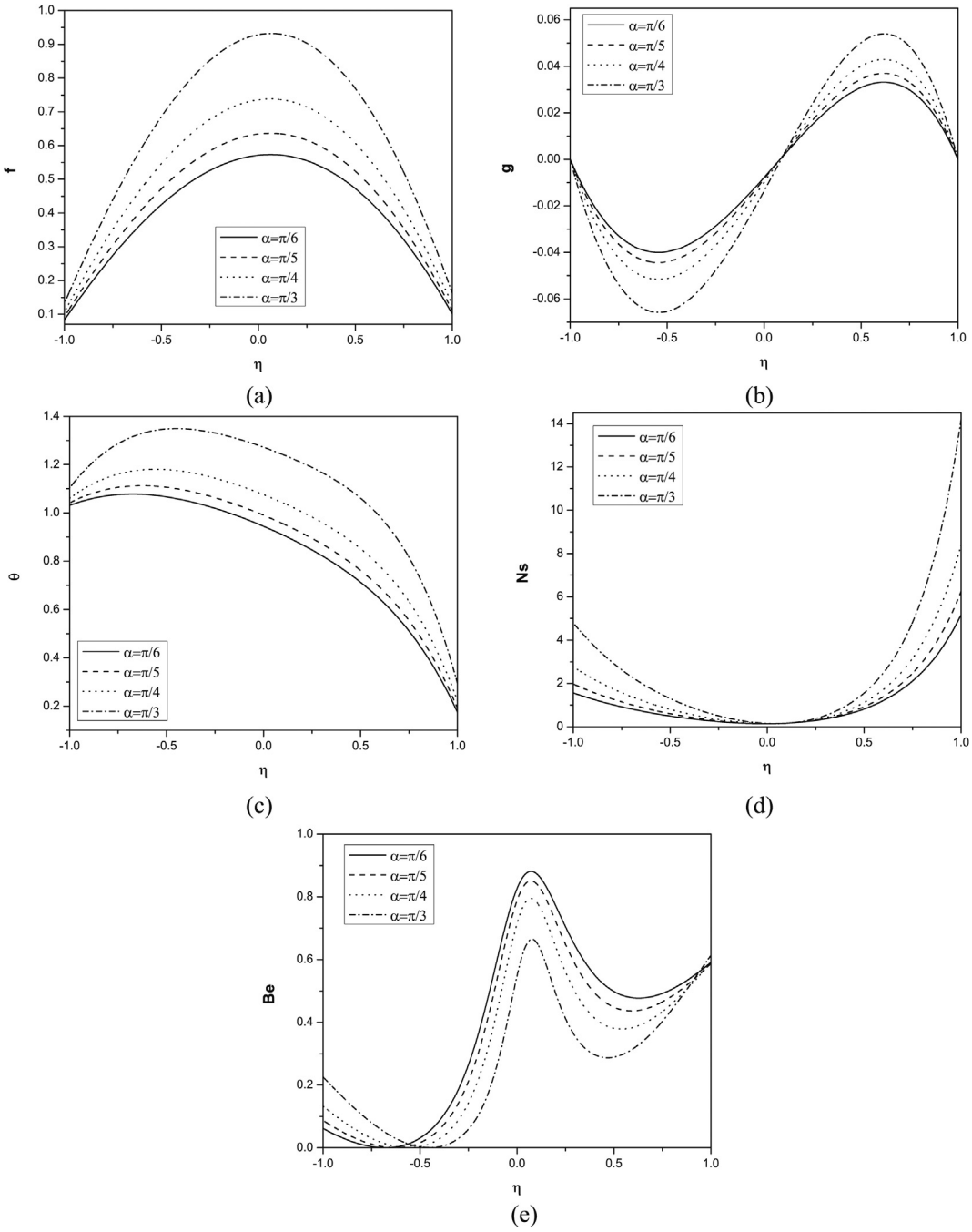

Fig. 3. Effect of angle of inclination on velocity, microrotation, temperature, entropy generation and Bejan number for $Pr = 1$, $N = 0.5$, $a_j = 0.001$, $Bi = 10$, $A = -1$, $\alpha_1 = 0.05$, $Re = 1$, $Br = 1$, $m = 1$, $Gr = 2$, $T_p = 1$, $R = 1$.

number *Br*, Reynolds number *Re* and Biot number *Bi* on the non-dimensional velocity, microrotation, temperature, entropy generation and Bejan number of the fluid flow through an inclined channel have been discussed.

In order to assess the accuracy of our method, we have compared our results with the analytical solution of Ariman and Cakmak [30] in the absence of R, α and α_1 with the fixed values of $N = 0.1$, $m = 1$ and $A = -1$. The comparison in the above case is found to be in good agreement, as shown in Table 1.

The effect of the coupling number on velocity, microrotation, temperature, entropy generation and Bejan number of the fluid flow through an inclined channel is plotted in Fig. 2(a)–(e). The coupling number N characterizes the coupling of linear and rotational motion arising from the micromotion of the fluid molecules. Hence N signifies the coupling between the Newtonian (μ) and rotational viscosities (κ) and hence $0 \leq N < 1$. Largest value of N, the effect of microstructure becomes significant and for the smallest value of N, the individuality of the substructure is less. As $\kappa \to 0$ i.e. $N \to 0$, the micropolarity is lost and the fluid behaves as non-polar fluid. Hence, $N \to 0$ corresponds to viscous fluid. Generally a parabolic velocity profile is observed, with maximum velocity along the channel centreline and minimum velocity at the plates.

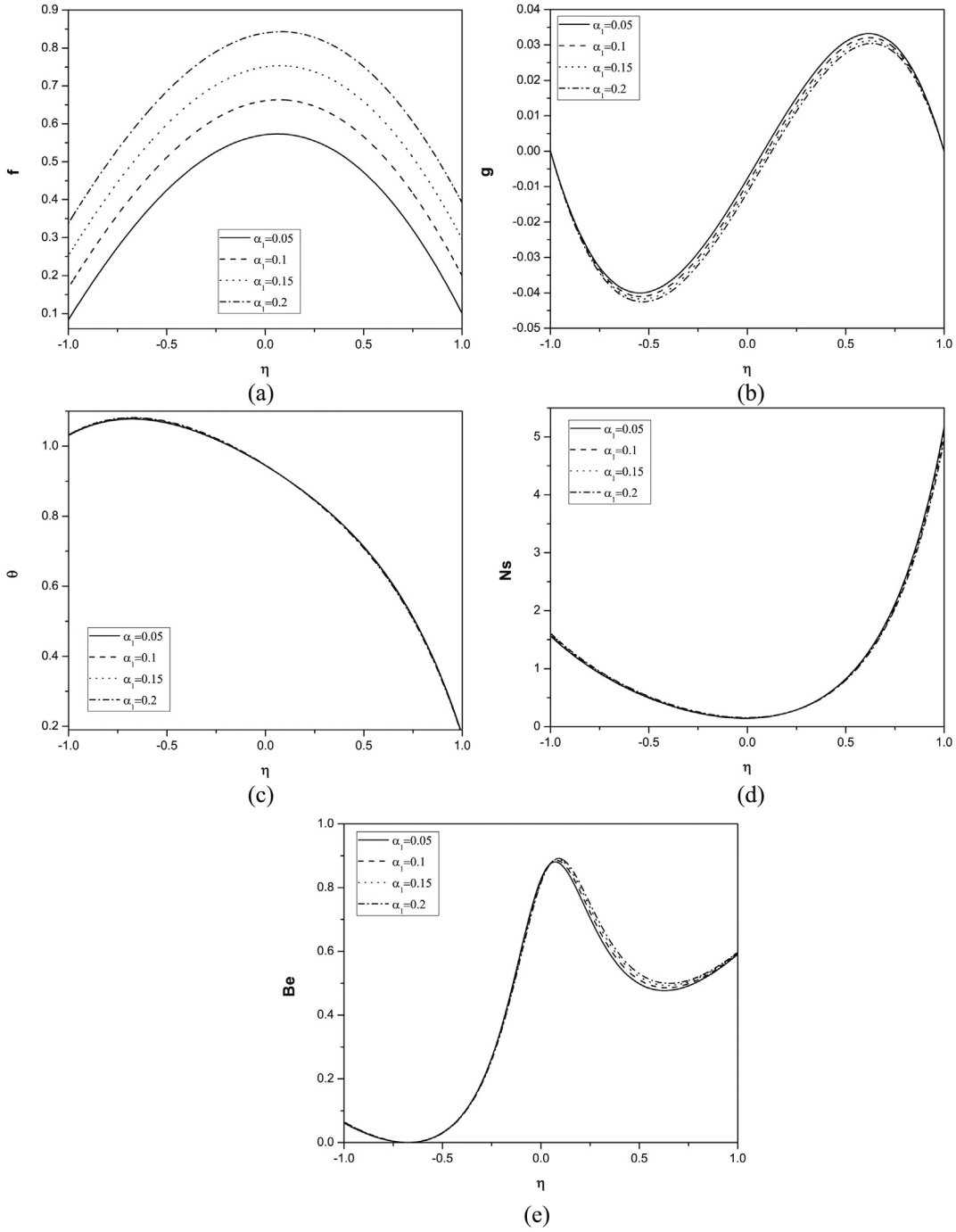

Fig. 4. Effect of slip parameter on velocity, microrotation, temperature, entropy generation and Bejan number for $Pr = 1$, $N = 0.5$, $a_j = 0.001$, $Bi = 10$, $A = -1$, $Re = 1$, $Br = 1$,$\alpha = \pi/6$, $m = 1$, $Gr = 2$, $T_p = 1$, $R = 1$.

It is observed from Fig. 2(a) that the velocity decreases with the increase of coupling number N. The peak velocity decreases in amplitude with an increase of N. The velocity for micropolar fluid case is less compared to viscous fluid case. It is seen from Fig. 2(b) that the microrotation component increases near the lower plate and decreases near the upper plate with increase in the value of coupling number N. It is observed from Fig. 2(c) and (d) that the temperature and entropy generation decreases with increase in the value of coupling number. It is clear from Fig. 2(e) that the Bejan number increases with increase in the value of N. We observe that heat transfer irreversibility dominates around the centreline region of the channel, and the fluid friction dominates at the lower plate.

Fig. 3 present the effect of angle of inclination α on velocity, microrotation, temperature, entropy generation and Bejan number. It is noticed from Fig. 3(a) that the velocity increases with the angle of inclination, due to increase in forces acting upon the fluid flow. It is shown from Fig. 3(b) that the microrotation component decreases near the lower plate and increases near the upper plate with an increase in the value of angle of inclination, showing a reverse rotation near the two boundaries. It is observed from Fig. 3(c) and (d) that the temperature and entropy generation

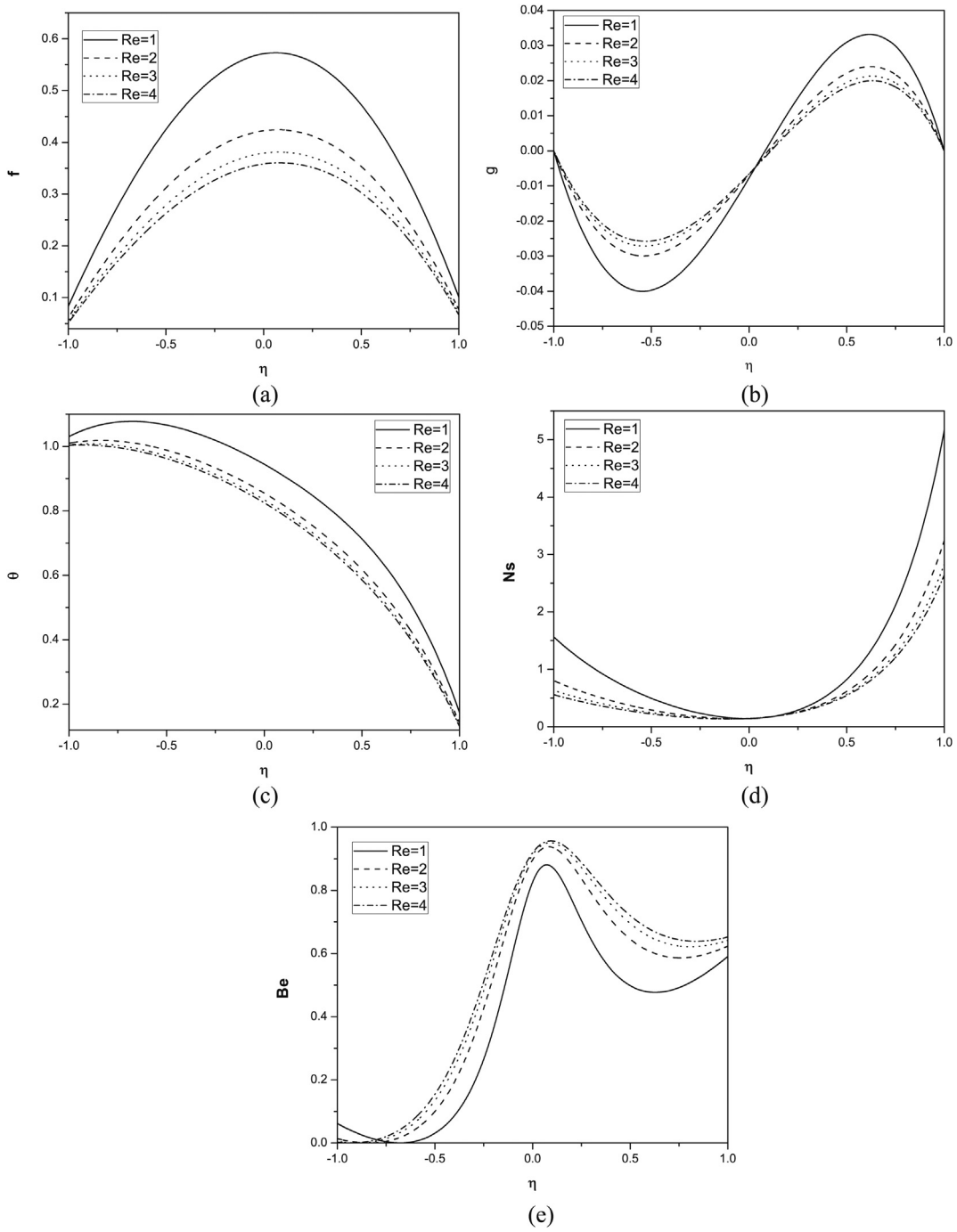

Fig. 5. Effect of Reynolds number on velocity, microrotation, temperature, entropy generation and Bejan number for $Pr = 1$, $N = 0.5$, $a_j = 0.001$, $Bi = 10$, $A = -1$, $\alpha_1 = 0.05$, $Br = 1$, $\alpha = \pi/6$, $m = 1$, $Gr = 2$, $T_p = 1$, $R = 1$.

increases with increase in the value of angle of inclination. We observe that the entropy-generation rate is less in the region around the channel centreline and increases quite rapidly to its maximum values at the upper plate of the channel for all the parameter variations. It is observed from Fig. 3(e) that the Bejan number decreases with increase in the value of α.

The variation of slip parameter on velocity, microrotation, temperature, entropy generation and Bejan number is displayed in Fig. 4. It is observed that the increase in slip parameter increases the velocity and decreases the microrotation as shown in Fig. 4(a) and (b). It is clear from Fig. 4(c) and (d) that there is no effect of slip parameter on temperature and entropy generation. The effect of slip parameter on Bejan number is shown in Fig. 4(e). It is observed that there is no significant effect up to center of the channel, but it increases near the upper plate.

The influence of Reynolds number on velocity, microrotation, temperature, entropy generation and Bejan number is shown in Fig. 5. From Fig. 5(a)–(d), we observe that as the Reynolds number increases, decreasing nature of velocity, microrotation (numerically), temperature and entropy generation is seen. Entropy generation number is high in magnitude near the upper plate due to the presence of high temperature and velocity gradients. Fig. 5(e)

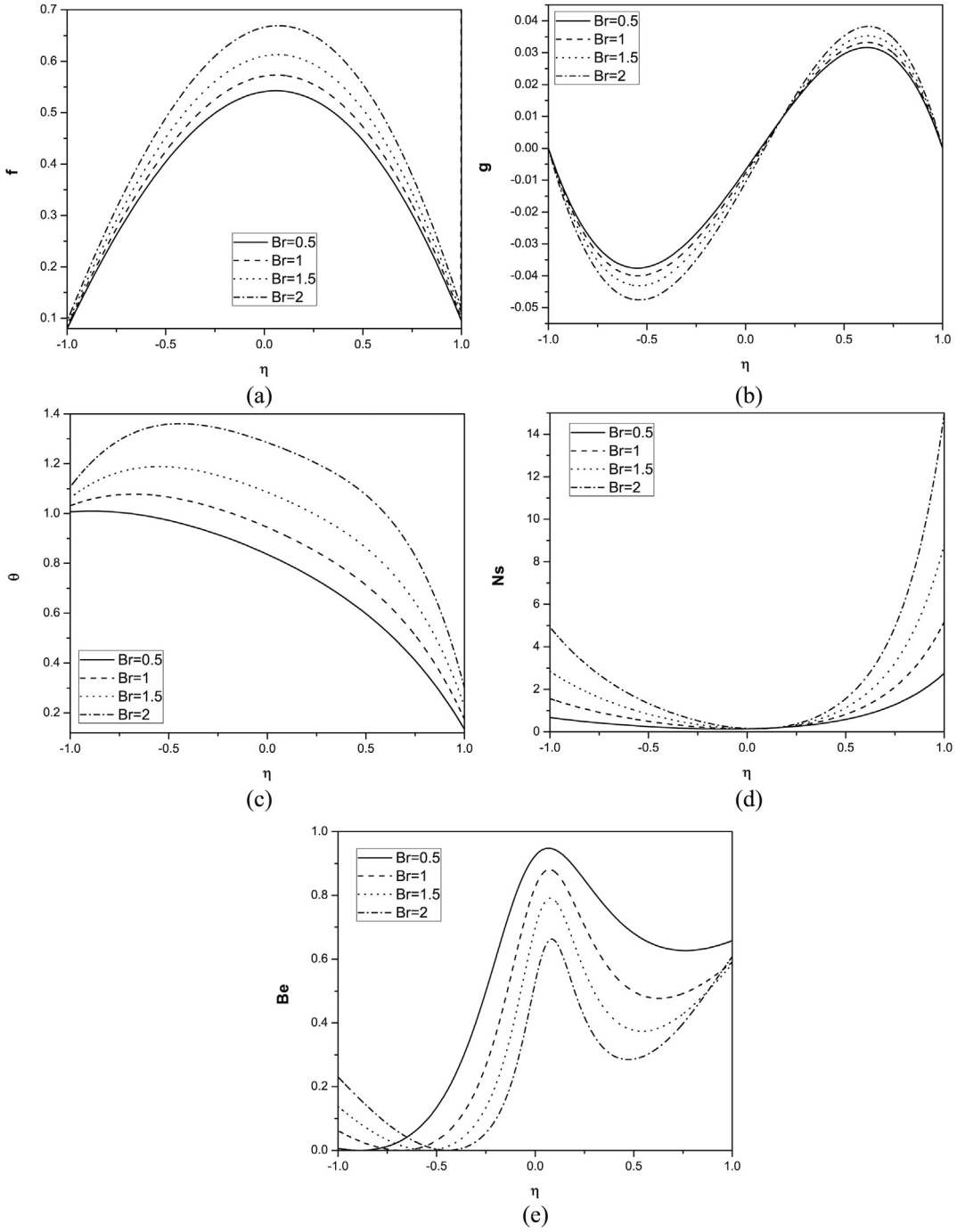

Fig. 6. Effect of Brinkman number on velocity, microrotation, temperature, entropy generation and Bejan number for $Pr = 1$, $N = 0.5$, $a_j = 0.001$, $Bi = 10$, $A = -1$, $\alpha_1 = 0.05$, $Re = 1$, $\alpha = \pi/6$, $m = 1$, $Gr = 2$, $T_p = 1$, $R = 1$.

shows that as Reynolds number increases, Bejan number increases. This implies that in the entire flow region, as *Re* increases the relative increase of dissipation of energy dominates the fluid friction.

The effect of Brinkman number on velocity, microrotation, temperature, entropy generation and Bejan number is displayed in Fig. 6. The parameter *Br* determines a relative importance of viscous effects and has a significant effect on entropy generation. Fig. 6(a) depicts that the non-dimensional velocity increases with increase in the value of Brinkman number. It is seen from Fig. 6(b) that the microrotation component decreases near the lower plate and increases near the upper plate with an increase in the value of Brinkman number. It is observed from Fig. 6(c) and (d) that the temperature and entropy generation increases with increase in the value of Brinkman number. The Brinkman number *Br* is indicative of the rate at which energy is dissipated by the viscous forces within the fluid. The reason for this effect entropy generation becomes significant in the region close to the channel walls. An increase in Brinkman number increases the fluid temperature (Fig. 6(c)) as well as temperature gradient within the channel. Consequently, as shown in Fig. 6(e), the dominance of fluid friction

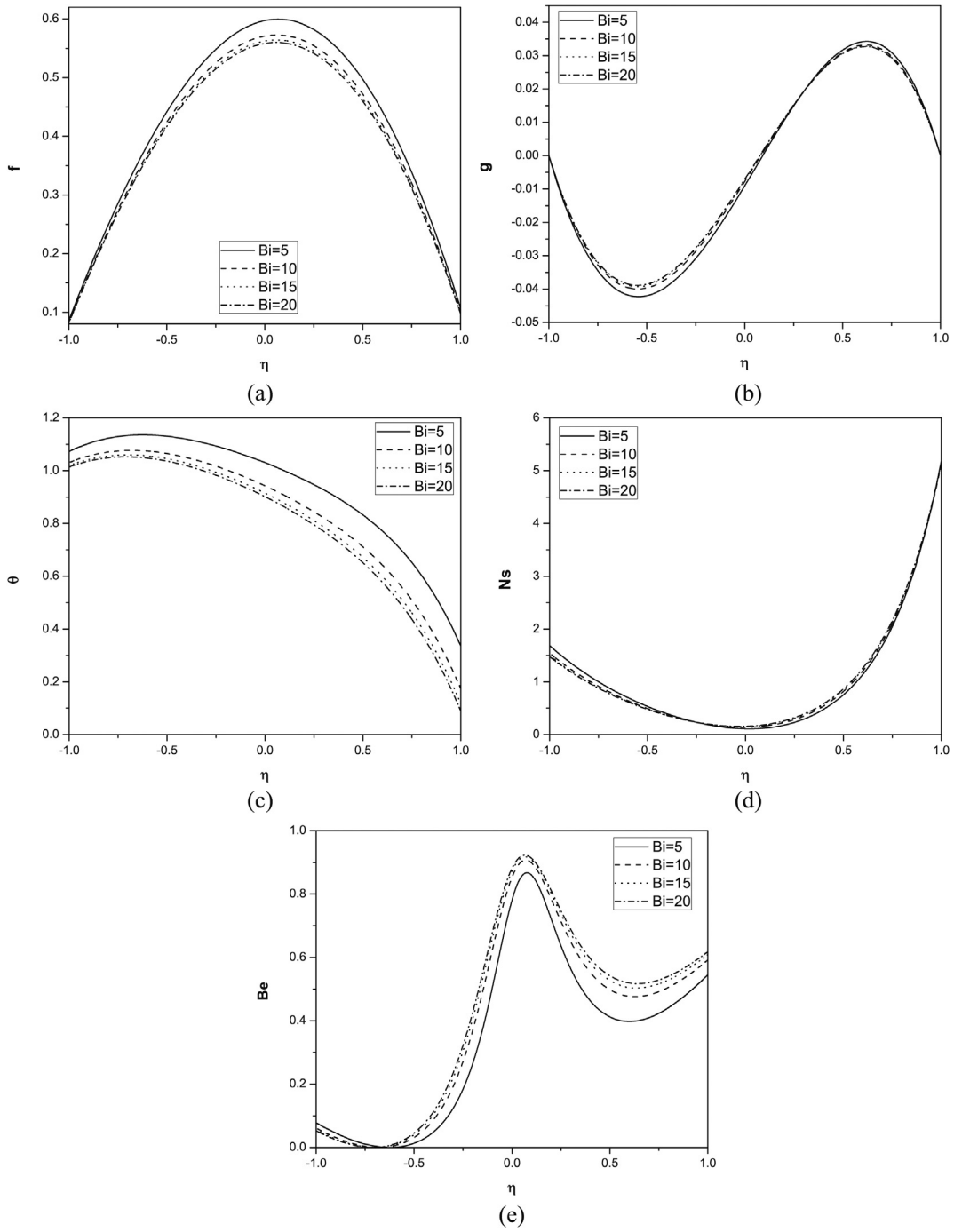

Fig. 7. Effect of Biot's number on velocity, microrotation, temperature, entropy generation and Bejan number for $Pr = 1$, $N = 0.5$, $a_j = 0.001$, $A = -1$, $\alpha_1 = 0.05$, $Re = 1$, $\alpha = \pi/6$, $m = 1$, $Gr = 2$, $T_p = 1$, $R = 1$.

Table 1
Comparison analysis for the velocity and microrotation calculated by the present method and that of analytical solution [30] for $R = 0$, $\alpha = 0$ and $\alpha_1 = 0$.

	Velocity $f(\eta)$		Microrotation $g(\eta)$	
η	Analytical solution [30]	Present	Analytical solution [30]	Present
−1	0	0	0	0
−0.8090	0.1557	0.1557	−0.0204	−0.0204
−0.6129	0.2817	0.2817	−0.0275	−0.0275
−0.4258	0.3696	0.3696	−0.0248	−0.0248
−0.2181	0.4302	0.4302	−0.0147	−0.0147
0	0.4518	0.4518	0	0
0.2181	0.4302	0.4302	0.0147	0.0147
0.4258	0.3696	0.3696	0.0248	0.0248
0.6129	0.2817	0.2817	0.0275	0.0275
0.8090	0.1557	0.1557	0.0204	0.0204
1	0	0	0	0

irreversibility over heat transfer irreversibility decreases with increase in *Br*.

The variation of velocity, microrotation, temperature, entropy generation and Bejan number with Biot's number is displayed in Fig. 7. The Biot number *Bi* is the ratio of internal thermal resistance of a solid to boundary layer thermal resistance. When Bi = 0 the plate is totally insulated internal thermal resistance of the plate is extremely high and no convective heat transfer to the cold fluid on the upper part of the plate takes place. Fig. 7(a) depicts that the non-dimensional velocity decreases with increase in the value of Biot's number. It is seen from Fig. 7(b) that the microrotation component increases near the lower plate and decreases near the upper plate with an increase in the value of Biot's number. It is observed from Fig. 7(c) that the temperature decreases with increase in the value of Biot's number. It is noticed from 7(d) that the entropy generation *Ns* decreases slightly with increase in the Biot's number. *Ns* profiles are similar in shape and are almost parallel to one another, for all the parameters, but they vary in magnitude. As the *Bi* increases the Bejan number increases as depicted in Fig. 7(e). Generally the Bejan number is highest along the channel center line region with irreversibility due to heat transfer dominating the flow, while near the channel walls the fluid friction irreversibility dominate.

6. Conclusions

Entropy generation in a micropolar fluid flow in an inclined channel with slip and convective boundary conditions is analyzed. The solutions are obtained numerically by applying spectral quasilinearization method. Some of the results obtained can be summarized as follows.

1. The velocity profiles increases with increase in α, α_1 and *Br*. The velocity decreases with increase in *N*, *Re* and *Bi*.
2. Fluid temperature increases with increasing α and *Br* and decreases with *N*, *Re* and *Bi*. There is no effect of slip parameter on fluid temperature.
3. The entropy generation rate increases at both the plates with increase in α and *Br* and it decreases at both the plates with increase in *N*, *Re*.
4. There is no change in the entropy generation at the center of the channel with increase in *N*, α, *Br* and *Re*.
5. All the Bejan number profiles show a minimum value at the lower plate and maximum value at the center of the channel.

7. Acknowledgment

The authors gratefully acknowledge the referees for their constructive comments and valuable suggestions.

References

[1] Bejan A. A study of entropy generation in fundamental convective heat transfer. J Heat Transf 1979;101:718–25.
[2] Bejan A. Second law analysis in heat transfer and thermal design. Adv Heat Transf 1982;15:1–58.
[3] Bejan A. Entropy generation minimization. New York: CRC Press; 1996.
[4] Makinde OD. Entropy-generation analysis for variable-viscosity channel flow with non-uniform wall temperature. Appl Energy 2008;85:384–93.
[5] Chen COK, Yang YT, Chang KH. The effect of thermal radiation on entropy generation due to micro-polar fluid flow along a wavy surface. Entropy 2011;13(9):1595–610.
[6] de Haro ML, Cuevas S, Beltrn A. Heat transfer and entropy generation in the parallel plate flow of a power-law fluid with asymmetric convective cooling. Energy 2014;66:750–6.
[7] Havzali M, Arikoglu A, Komurgoz G, Keser HI, Fraser RO. Analytical numerical analysis of entropy generation for gravity-driven inclined channel flow with initial transition and entrance effects. Phys Scr 2008;78. 1–7, 045401.
[8] Kamisli F, Oztop HF. Second law analysis of the 2D laminar flow of two-immiscible, incompressible viscous fluids in a channel. Heat Mass Transf 2008;44:751–61.
[9] Cimpean DS, Pop I. A study of entropy generation minimization in an inclined channel. Wseas Trans Heat Mass Transf 2011;06:31–40.
[10] Komurgoz G, Arikoglu A, Ibrahim O. Analysis of the magnetic effect on entropy generation in an inclined channel partially filled with a porous medium. Numer Heat Transf 2012;61(A):786–99.
[11] Damseh RA, Al-Odat MQ, Al-Nimr MA. Entropy generation during fluid flow in a channel under the effect of transverse magnetic field. Heat Mass Transf 2013;44:897–904.
[12] Eegunjobi AS, Makinde OD. Entropy generation analysis in a variable viscosity MHD channel flow with permeable Walls and convective heating. Math Problems Eng 2013;2013:1–12.
[13] Das S, Jana RN. Entropy generation due to MHD flow in a porous channel with Navier slip. Ain Shams Eng J 2014;5:575–84.
[14] Mahdavi M, Saffar-Avval M, Tiari S, Mansoori Z. Entropy generation and heat transfer numerical analysis in pipes partially filled with porous medium. Int J Heat Mass Transf 2014;79:496–506.
[15] Torabi M, Zhang K, Yang G, Wang J, Wu P. Heat transfer and entropy generation analyses in a channel partially filled with porous media using local thermal non-equilibrium model. Energy 2015;82:922–38.
[16] Torabi M, Zhang K. Temperature distribution, local and total entropy generation analyses in MHD porous channels with thick walls. Energy 2015;87:540–54.
[17] Navier CLM. Sur les lois du mouvement des fluides. Mem Acad Royale des Sci 1827;6:389–440.
[18] Denn MM. Issues in viscoelastic fluid mechanics. Annu Rev Fluid Mech 1990;22:13–32.
[19] Denn MM. Extrusions instabilities and wall slip. Annu Rev Fluid Mech 2001;33:265–87.
[20] Iman Z. On the importance of thermal boundary conditions in heat transfer and entropy generation for natural convection inside a porous enclosure. Int J Therm Sci 2008;47:339–46.
[21] Hooman K. Heat transfer and entropy generation for forced convection through a microduct of rectangular cross-section: effects of velocity slip, temperature jump, and duct geometry. Int Commun Heat Mass Transf 2008;35:1065–8.
[22] Butt AS, Munawar S, Ali A, Mehmood A. Entropy generation in hydrodynamic slip flow over a vertical plate with convective boundary. J Mech Sci Technol 2012;26(9):2977–84.
[23] Chinyoka T, Makinde OD. Analysis of entropy generation rate in an unsteady porous channel flow with navier slip and convective cooling. Entropy 2013;15:2081–99.

[24] Anand V. Slip law effects on heat transfer and entropy generation of pressure driven flow of a power law fluid in a microchannel under uniform heat flux boundary condition. Energy 2014;76:716–32.
[25] Mostafa S, Ali K. Convective heat transfer and entropy generation analysis on Newtonian and non-Newtonian fluid flows between parallel-plates under slip boundary conditions. Int J Heat Mass Transf 2014;70:664–73.
[26] Ibanez G. Entropy generation in MHD porous channel with hydrodynamic slip and convective boundary conditions. Int J Heat Mass Transf 2014;80:274–80.
[27] Eringen AC. The theory of micropolar fluids. J Math Mech 1966;16:1–18.
[28] Bellman RE, Kalaba RE. Quasilinearisation and non-linear boundary-value problems. New York, NY, USA: Elsevier; 1965.
[29] Canuto C, Hussaini MY, Quarteroni A, Zang TA. Spectral methods fundamentals in single domains. Springer Verlag; 2006.
[30] Ariman T, Cakmak AS. Some basic viscous flows in micropolar fluids. Rheol Acta 1968;7(3):236–42.